JOURNAL OF PROPULSION AND POWER
Vol. 21, No. 5, September–October 2005

Design and Test of a Hypersonic Isentropic-Spike Intake with Aligned Cowl

A. J. Matthews* and T. V. Jones†
University of Oxford, Oxford, England OX1 3PJ, United Kingdom
and
T. M. Cain‡
QinetiQ, Ltd., Farnborough, England GU14 0LX, United Kingdom

A study of reexpansion scramjet intakes is presented. Reexpansion intakes employ mixed external-internal compression with the internal contraction fixed by starting requirements and a cowl aligned with the external flow to minimize intake contribution to vehicle drag. As a result of the starting limitation, the captured flow is partially reexpanded, resulting in nonuniform flow at the intake exit. Stream thrust averaging was used to determine equivalent one-dimensional flow for input to a scramjet engine cycle analysis. Engine performance increases with compression, and thus optimum turning-angle appears to be at the limit for detachment of the internal cowl shock. An axisymmetric reexpansion intake was built using stereo lithography and tested at Mach 7.1 in the University of Oxford gun tunnel. The stream-thrust-averaged properties were determined experimentally from measurements of axial force and mass capture. Schlieren and surface-pressure measurements were taken. Skin friction in the model isolator section was found to significantly affect intake performance, increasing the amount of compression and reducing efficiency. Starting characteristics were determined experimentally in QinetiQ's High Density Tunnel.

Nomenclature

A	=	area, m^2
C_T	=	thrust coefficient, $F_T/\frac{1}{2}\rho_1 v_1^2 A_e$
D_∞	=	capture diameter, m
$E1$	=	engine cycle with nozzle expansion $p_e/p_1 = 1$
$E2$	=	engine cycle with nozzle expansion $A_e/A_\infty = 2$
F	=	force, N
g	=	acceleration caused by gravity, m/s^2
h	=	specific enthalpy, referenced to 25°C, J/kg
I	=	specific impulse, $F_T/\dot{m}_{H2}g$, s
k_s	=	roughness, m
M	=	Mach number
$\dot{m}$	=	mass flow rate, kg/s
p	=	pressure, Pa
p_{02}/p_{01}	=	total pressure recovery
Q	=	heat transfer, W
Re_D	=	Reynolds number, $\rho_1 v_1 D_\infty/\mu_1$
T	=	temperature, K
v	=	velocity, m/s
x	=	distance, m
γ	=	ratio of specific heats
η_{KE}	=	kinetic energy efficiency, $[h_{02} - h(p_1, s_2)]/(h_{01} - h_1)$
θ_1	=	intake initial cone/wedge angle, deg
θ_2	=	intake final wall slope, deg
μ	=	dynamic viscosity, Pa s
ρ	=	density, kg/m^3

Subscripts

add	=	additive drag
bp	=	base pressure
c	=	cowl closure plane
cd	=	cowl drag
e	=	scramjet engine exit plane
exd	=	external drag
f	=	frictional force
geo	=	geometric
$H2$	=	hydrogen
I	=	isolator
inv	=	inviscid
LC	=	load cell
p	=	pressure force
pl	=	plenum
s	=	surface area
T	=	thrust
w	=	wall
x	=	axial force, cross-sectional area
0	=	total conditions
1	=	captured flow free stream conditions
2	=	mixed to uniform conditions at intake exit
∞	=	full mass capture freestream conditions

Presented as Paper 2003-7045 at the AIAA 12th International Space Planes and Hypersonic Systems and Technologies, Norfolk, VA, 15–19 December 2003; received 1 September 2004; revision received 27 January 2005; accepted for publication 29 January 2005.

*Departmental Lecturer, Department of Engineering Science, Parks Road.
†D. Schultz Professor of Turbomachinery, Department of Engineering Science, Parks Road.
‡QinetiQ Fellow, 1079/A7 Building, Ively Road.

Introduction

THE intake of a hypersonic engine is required to capture and efficiently compress air so that after heat addition the flow can be expanded in the nozzle to produce thrust. Design criteria for a hypersonic intake have been well documented in the literature.[1–3] In summary form, the following is true:

1) The intake should compress the flow as efficiently as possible, minimizing viscous losses and shock-wave losses.

2) Intake contribution to vehicle drag should be minimized.

3) The intake should be self-starting at the scramjet takeover Mach numbers ($M_1 \sim 4$) and be able to operate over the required range of Mach numbers, with no significant deterioration in performance.

4) Intake performance should not be significantly reduced by operation at incidence.

5) The intake must be able to tolerate the backpressures caused by heat addition.

6) The intake has to be able to withstand the internal pressures and heat loads.

7) Uniform velocity profiles are generally desirable at the intake exit.

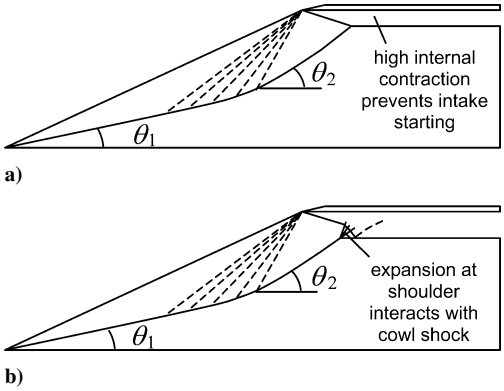

Fig. 1 Schematic diagram of: a) Ideal low-drag intake and b) REX intake.

An intake concept that should satisfy the first six criteria is explored here. The nonuniform flow it delivers to the combustor complicates the performance assessment but is not necessarily detrimental to combustor performance.

Reexpansion Intake Design

Figure 1a shows a schematic diagram of a mixed-compression, ideal, low-drag intake. The cowl is aligned with the external flow to minimize drag, and the captured flow is realigned through a single oblique shock wave. The performance of such intakes can be high; however, they are not self-starting except for the case of very low compression. Figure 1b shows a schematic diagram of a reexpansion (REX) intake, which was designed by opening the throat of the ideal low-drag intake sufficiently to ensure self-starting. As a result, internal expansions are introduced that decrease intake efficiency and increase nonuniformity.

Two-dimensional and axisymmetric REX intakes are designed with an initial wedge or cone compression followed by isentropic compression through a fan focused at the cowl lip. Taylor–Maccoll and the method of characteristics were used to calculate the axisymmetric cases. The inviscid contours were corrected for boundary-layer displacement obtained from the momentum integral method. Skin friction was calculated from a turbulent flat-plate correlation based on momentum thickness with properties evaluated at Eckert's reference temperature.[4] Constant values 0.9 and 0.8 were assumed for the recovery factor and Reynolds analogy factor, respectively.[5] Stollery's flat-plate correlation for shape factor was used.[6] The intake surface was assumed to be at uniform temperature calculated by integrating heat transfer over the compression surface and equating this to the radiation from the surface, assuming an emissivity of 0.8.

The cross-sectional area of the inviscid throat was set equal to the limiting value for self-starting by applying the Kantrowitz and Donaldson starting criterion.[7] This assumes that at the limiting internal contraction the subsonic flow downstream of a normal shock wave situated at the cowl closure plane accelerates to Mach 1 at the intake throat. To account for the nonuniform flow in the axisymmetric case, the cowl closure plane was taken to be the curved surface originating from the cowl that is at all points normal to the flow. A normal shock wave following this curved surface creates a nonuniform subsonic flow. Incremental areas of this subsonic flow were assumed to accelerate independently and one dimensionally to Mach 1. The sum of the incremental areas at Mach 1 was taken to be the limiting Kantrowitz throat. Adding the boundary-layer displacement thickness determined for the started intake as just described above results in a geometric contraction ratio somewhat less than the inviscid value. It is recognized that the boundary layer in the unstarted condition bears no resemblance to that with the design flow, and an experiment is required to determine the maximum self-starting internal-contraction ratio.

Intake Performance

The performance of a hypersonic intake is characterized in terms of the amount of compression performed (intake capability), the efficiency of the diffusion process, mass capture, and contribution to vehicle drag. Many different intake performance parameters have been defined and investigated.[8–10] Mölder and McGregor[10] suggest the best way to assess an intake is to couple it to an ideal combustor and nozzle and calculate engine performance. This has the advantage of incorporating additive drag and cowl drag into the assessment. Andreev and Penzin[11] went further and modelled vehicle performance over the desired trajectory in order to account for variation in mass capture and efficiency over the Mach-number range. Single point performance is unlikely to be the only design driver.

Nonuniform flow at the intake exit presents a problem for the generally one-dimensional methods used to calculate combustor and nozzle performance. One-dimensional representation that conserves the mass flow, momentum, and energy of the true flowfield is sometimes referred to as stream-thrust-averaged flow.[3] It is calculated using a control volume analysis, with nonuniform intake flow entering one end of a constant-area frictionless duct, and a fully mixed-out uniform flow exiting the other.

Stream-thrust-averaged intake efficiencies appear low when compared to those calculated using other nonphysical approaches such as mass or area averaging. In part this is because of the introduction of mixing losses that might more rightly be attributed to the combustor. Mixing losses are necessary to disperse and mix the fuel with the air on a molecular level, and nonuniform inlet conditions can contribute to this process. Here, an ideal combustor is assumed, and the mixing losses must be attributed to the intake.

Figure 2 shows the captured flow control volume. The conservation equations are given by Eqs. (1) to (3):

Continuity:

$$\dot{m}_1 = \rho_1 A_1 v_1 = \rho_2 A_{2\text{geo}} v_2 \tag{1}$$

Momentum:

$$p_1 A_\infty - p_2 A_{2\text{geo}} - F_x = \dot{m}_1 v_2 - \dot{m}_1 v_1 \tag{2}$$

Energy:

$$h_1 + v_1^2/2 - Q/\dot{m}_1 = h_2 + v_2^2/2 \tag{3}$$

The axial force $F_x = F_p + F_f - F_{\text{add}}$ comprises the axial component of the pressure force and frictional force acting on the compression surface and the additive drag defined as

$$F_{\text{add}} = \int_{A_1}^{A_\infty} (p_{\text{add}} - p_1)\, \mathrm{d}A_x \tag{4}$$

where $\mathrm{d}A_x$ is the axial projection of an area element. Knowing the freestream conditions, $A_{2\text{geo}}$, $\dot{m}_1$, F_x, and Q, Eqs. (1–3) and the equation of state $p_2 = \rho_2 R T_2$ are solved iteratively for T_2, v_2, ρ_2, and p_2.

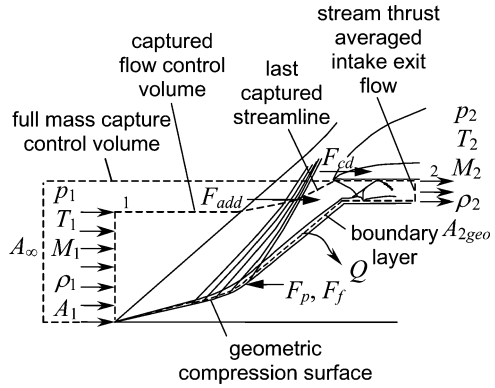

Fig. 2 Captured flow control volume for a geometric intake.

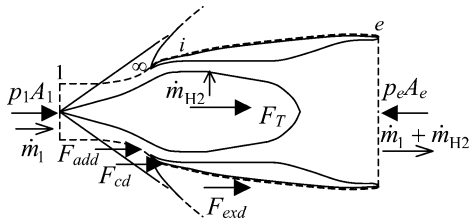

Fig. 3 Engine control volume.

Engine Cycle Analysis

The engine control volume is shown in Fig. 3. The thrust F_T was calculated from

$$F_T = (\dot{m}_1 + \dot{m}_{H2})v_e - \dot{m}_1 v_1 + (p_e - p_1)A_e - F_{\text{add}} - F_{\text{cd}} \quad (5)$$

where

$$F_{\text{cd}} = \int_{A_\infty}^{Ai} (p_{\text{cd}} - p_1)\ \mathrm{d}A_x + F_{f\text{cd}}$$

and F_{add} is defined by Eq. (4). The cowl is taken to be that part of the external body upstream of location i, at which the internal flow is realigned with the axis. For the case of REX intakes, cowl drag only arises because of the structural thickness of the cowl. The external drag on the remainder of the body

$$F_{\text{exd}} = \int_{A_i}^{A_e} (p_{\text{exd}} - p_1)\ \mathrm{d}A_x + F_{f\text{exd}}$$

is allocated to the airframe (setting $p_{\text{exd}} = p_1$ and $F_{f\text{exd}} = 0$) and hence is not subtracted from the engine thrust. This method of bookkeeping helps in optimizing performance of highly integrated engine/airframes.[12]

Exhaust velocity and pressure are calculated with the following assumptions: 1) combustor entry flow conditions are the stream-thrust-averaged intake exit properties; 2) hydrogen fuel is injected normal to the engine axis at stoichiometric conditions; 3) combustor exit area is such that the flow is thermally choked at the combustor exit; 4) pressure is assumed to vary linearly with area within the combustor; 5) combustor heat loss and skin friction are zero; 6) the mixture is in chemical equilibrium within the combustor; and 7) the mixture is either in equilibrium or frozen within the nozzle. Mixture properties were calculated using the NASA-Lewis Chemical Equilibrium Program.[13] Two engines were considered: $E1$, in which flow is expanded in the nozzle back to ambient pressure ($p_e = p_1$), and $E2$, in which the nozzle-exit area is fixed at $A_e/A_\infty = 2$. Engine performance is presented in terms of the engine thrust coefficient based on A_e and the specific impulse.

Calculated REX Performance

Calculated stream-thrust-averaged capability parameters of axisymmetric REX intakes at Mach 7, $Re_D = 1.57 \times 10^6$ are presented in Fig. 4. The inviscid total contraction $A_1/A_{2\text{inv}}$ is also shown, represented by the dotted lines. The performance of two-dimensional REX intakes (not shown) was similar to that of axisymmetric REX intakes except that there is greater compression for a given flow deflection.

Efficiency parameters are presented in Fig. 5. The dotted lines represent inviscid adiabatic intakes, and the solid lines represent viscous intakes. Flow viscosity reduces the performance of these intakes through two independent mechanisms:

1) Skin friction contributes as an additional drag force acting on the intake. The effect of this is more apparent in the longer intakes with larger wetted areas.

2) The geometric contraction ratio is reduced as a consequence of applying a boundary-layer correction to account for the physical displacement of the inviscid flowfield. The effect of this is greater in intakes with higher contraction ratios (see Fig. 4), where

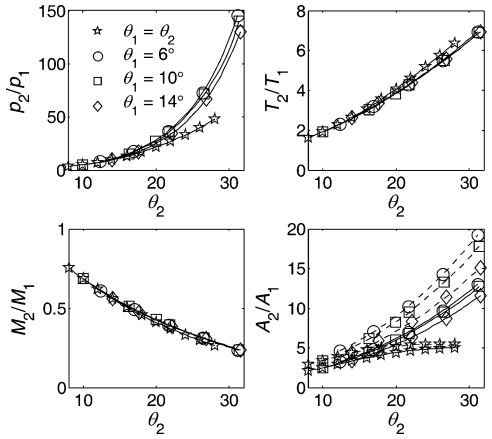

Fig. 4 Capability parameters.

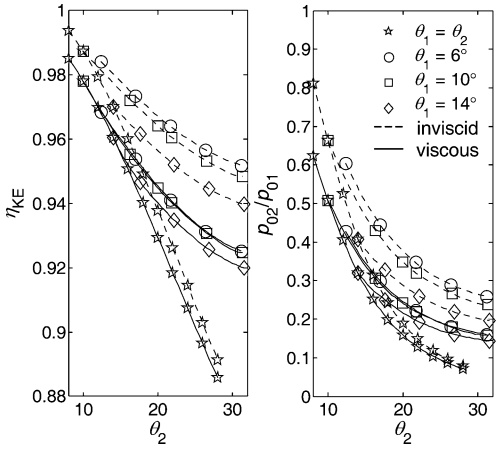

Fig. 5 Efficiency parameters.

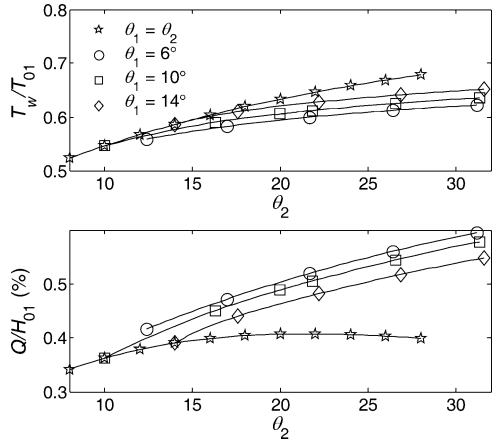

Fig. 6 Mean wall temperatures and heat transfer for radiatively cooled REX intakes.

the boundary-layer displacement thickness is large compared to the throat height.

Wall temperatures and total heat loss are shown in Fig. 6. The figure shows that at $M_1 = 7$ the heat transfer over the compression surface is small compared to the total enthalpy of the external flow. This implies that moderate inaccuracies in Q will not have a significant influence on the stream-thrust-averaged performance estimates.

Engine cycle performance is presented in Fig. 7. The solid lines represent equilibrium nozzle flow, and the dotted lines represent frozen nozzle flow. The graphs on the left are for $E1$, and the graphs on the right are for $E2$. In $E2$ both C_T and I are linearly proportional

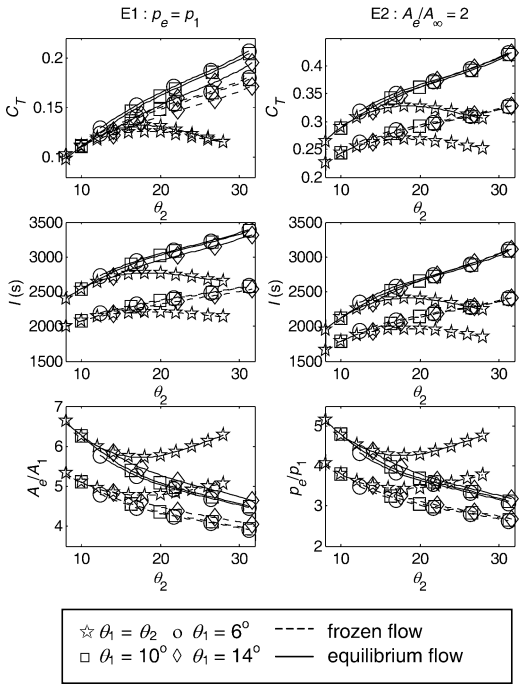

Fig. 7 Engine performance *E*1 (left) and *E*2 (right).

to thrust because the equivalence ratio and exit area are constant. The thrust coefficients of $E2$ are significantly higher than $E1$ and closer to what is probably required to balance drag and certainly much more appropriate for acceleration. The restricted area ratio implies that the capture area must be a high fraction of the projected vehicle area. Noting that specific impulse increases with compression at a greater rate for $E2$ than it does for the matched pressure engine $E1$, it becomes clear REX intakes need to be designed with high compression. Only in the case of a conical intake with no additional isentropic compression is there an optimum angle θ_2 (18 deg). With isentropic compression the initial cone angle has little effect on I with $6 \text{ deg} < \theta_1 < 14$ deg.

Experimental Program

An axisymmetric REX intake model (REX1020) in Fig. 8 was designed and tested in the University of Oxford gun tunnel at $Re_D = 2.0 \times 10^6$ with $T_w/T_{01} \approx 0.47$ over the compression surface. The gun tunnel produced Mach 7.1 flow through a contoured nozzle for 60 ms, attaining constant stagnation pressure for the last 20 ms of the run at nominal pressure $p_{01} = 6.34$ MPa. The nominal stagnation temperature $T_{01} = 720$ K was calculated from the measured pressure history in the gun tunnel barrel accounting for entropy increase across shocks and applying a 15% reduction to account for the heat transfer measured by Buttsworth and Jones.[14] The inviscid REX1020 flowfield was designed with initial 10-deg cone angle followed by isentropic compression to 20 deg at the wall, with all forebody waves focused at the cowl lip at $M_1 = 7.1$ and 100-mm capture diameter. The inviscid internal contraction was fixed at its limit for self-starting at Mach 7.1, $A_c/A_{2\text{inv}} = 1.522$. The intake contour was corrected for turbulent boundary-layer displacement calculated for the test conditions using the momentum integral method, which reduced the internal contraction by 10%. With six 2-mm-thick struts included to hold the cowl in place, the geometric contraction was $A_c/A_{2\text{geo}} = 1.507$, ~1% below the calculated limiting contraction. Manufacture by stereo lithography allowed incorporation of a network of complex tubing for multiple pressure tappings. The model was built without boundary-layer trips. The dural cowl and struts were bonded to the centerbody using a two-part adhesive. The cowl is 1.7 mm thick, with 15-deg external chamfer. A 0.5-mm-diam pitot-pressure tap is built into the nose tip. The model has a 5-mm radius transition from the compression surface to the throat. The isolator length is ~5.5 hydraulic diameters.

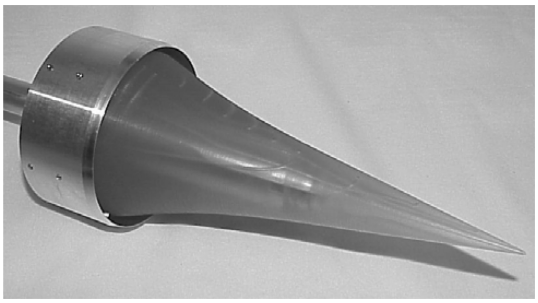

Fig. 8 REX1020 intake model.

The stream-thrust-averaged flow delivered by the intake was determined by measuring F_x and $\dot{m}_1/\dot{m}_\infty$. Heat flux is small in comparison with the total enthalpy of the gun tunnel flow and therefore could be calculated with sufficient accuracy for the purpose of determining stream-thrust-averaged quantities.

Axial-Force Measurement

The intake model was mounted on a hollow sting fitted with strain gauges. Each gauge was supplied by constant current, and the individual gauge voltages were numerically combined such that bending strains cancelled to give a linear response to axial force. The measured force comprised axial components caused by cowl drag, additive drag, isolator drag, and the base pressure force, as shown in Eq. (6):

$$F_{\text{LC}} = F_x + F_{\text{cd}} + F_{\text{add}} + F_I - F_{\text{bp}} \tag{6}$$

Isolator drag was found to be significant compared to F_x and was incorporated into intake performance. $F_x + F_I = 122 \pm 5.6$ N was determined from the following: 1) the measured axial force $F_{\text{LC}} = 125 \text{ N} \pm 2.2$ N; 2) F_{cd} estimated to be 7.4 N using laminar flat-plate values of skin friction and the Rankine–Hugoniot shock-wave relations to determine pressure on the 15-deg leading edge; 3) base drag estimated to be 4.3 N by assuming $p_{\text{bp}} = p_1/2$; and 4) F_{add} assumed zero because of near full mass capture.

Mass-Flow Measurement

The captured flow was dumped into a plenum attached to the base of the model before being exhausted through six sonic orifices of total area A^* in the plenum base plate. An annular wedge directed the flow from the intake towards the center of the plenum before it passed through a grid intended to produce uniform flow upstream of the choked orifices. Plenum stagnation pressure was measured at two radial locations. Intake mass capture was expressed as

$$\dot{m}_1/\dot{m}_\infty = K_{\dot{m}}\left(A^*/D_\infty^2\right)(p_{0\text{pl}}/p_{01}) \tag{7}$$

with $K_{\dot{m}}$ determined by calibration using two pitot intakes of different D_∞ but with identical exits to the REX1020 to provide known capture areas (mass flows). Unfortunately, flow in the plenum was nonuniform, and pressure at the two locations differed by around 10%.

An alternative estimate was obtained from the schlieren photograph shown in Fig. 9. The last captured streamline was determined from the shock-wave angle and indicates $\dot{m}_1/\dot{m}_\infty = 0.99 \pm 0.01$.

Experimental Results

The intake was tested in the gun tunnel at incidence up to 8 deg. At this limit the flow separated from the leeward compression surface 50 ms into the run. The flow remained attached to the windward surface throughout the run. Figures 9–11 show schlieren photographs of the REX1020 at 0, 4, and 8 deg (before unstart), respectively. Figure 12 shows the measured pressure distribution at various angles of incidence. The line at $x = 0.208$ m indicates the axial location of the cowl lip. The solid line is the calculated pressure distribution at 0-deg incidence and is approximately 10% lower than measured.

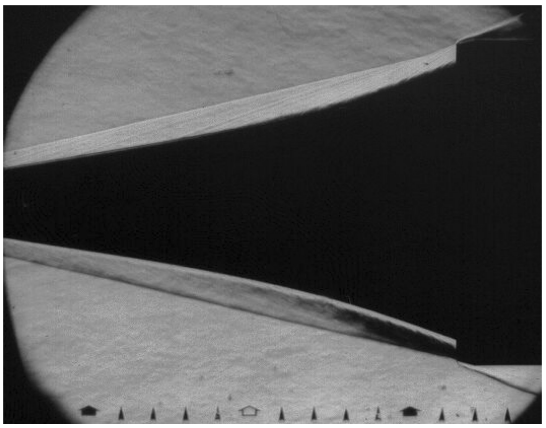

Fig. 9 Schlieren photograph of the REX1020 intake at 0-deg incidence.

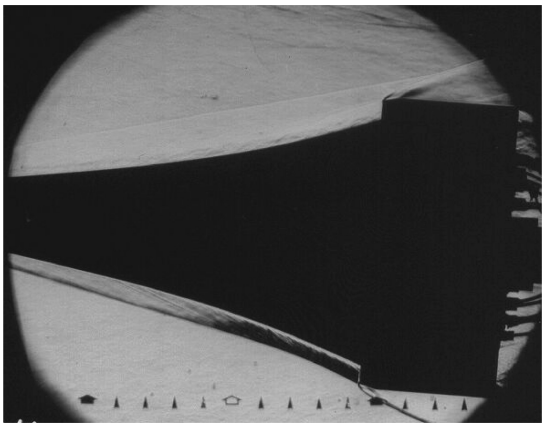

Fig. 10 Schlieren photograph of the REX1020 intake at 4-deg incidence.

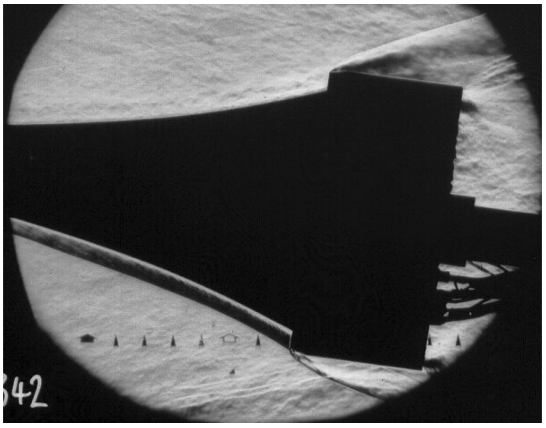

Fig. 11 Schlieren photograph of the REX1020 intake at 8-deg incidence prior to unstart.

The surface roughness at the conical part of the REX1020 is 24 μm, giving a roughness Reynolds number of $\rho_m v_\delta k_s/\mu_m \approx 80$ with the temperature-dependent flow properties evaluated at Eckert's reference temperature.[4] This corresponds to a hydraulically smooth surface when compared to Feindt's[15] transition data for distributed roughness in incompressible flow. In the absence of measurements to detect transition, an approximation is made using data collected by Schneider[16] to give $\rho_\delta v_\delta x_T/\mu_\delta \approx 5 \times 10^6$ for smooth cones in compressible flow, which predicts transition for the REX1020 around the start of the isentropic compression contour. It is difficult to detect evidence of transition on the schlieren photographs.

Table 1 REX1020 measured stream-thrust-averaged flow

Property	Value
p_2/p_1	45.0 ± 3.0
T_2/T_1	4.99 ± 0.25
M_2/M_1	0.341 ± 0.014
$A_1/A_{2\text{geo}}$	6.950
η_{KE}	0.91 ± 0.01
Q/H_{01}	$1.8 \pm 1\%$

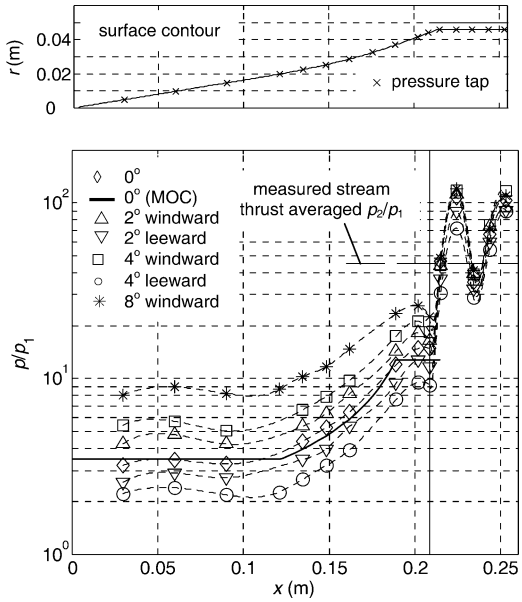

Fig. 12 Measured pressure distribution at incidence.

Stream-Thrust-Averaged Intake Performance

Measured stream-thrust-averaged quantities are presented in Table 1. The measured intake capability (compression) is significantly higher than calculated, and the measured intake efficiency is significantly lower. This is attributed mainly to the drag in the isolator section, which was not included in the intake performance calculations.

To account for viscous effects in the isolator in the control volume analysis, a net coefficient of skin friction is assumed based on the stream-thrust-averaged dynamic pressure and isolator surface area $C_{fI} = F_I/\frac{1}{2}\rho_2 v_2^2 A_{sI}$. The momentum equation (2) becomes

$$p_1 A_\infty - p_2 A_2 - F_x = \left(1 + \frac{2C_{fI} L_I}{D_{hI}}\right)\dot{m}_1 v_2 - \dot{m}_1 v_1 \qquad (8)$$

where L_I and D_{hI} are the isolator length and hydraulic diameter, respectively. In the energy equation (3), $Q = Q_{\text{cs}} + Q_I$, where Q_{cs} is the heat transfer integrated over the compression surface and Q_I is the heat transfer in the isolator. Iteration was used to solve Eqs. (1), (3), and (8) with the equation of state for a given value of C_{fI}. Isolator wall temperature was calculated from the corresponding heat flux by treating the model as semi-infinite.

The measured stream-thrust-averaged values correspond to an average isolator skin-friction coefficient of $C_{fI} \approx 0.005$. This is in agreement with that calculated from fully developed pipe flow theory, obtained by area averaging the skin-friction coefficients caused by the 15-μm roughness of the stereo lithography inner body and the 2.5-μm roughness of the dural cowl and struts. The corresponding calculated isolator drag $F_I = 32$ N is in reasonable agreement with the measured force $(F_x + F_I) = 122$ N, calculated skin friction $F_f \approx 10$ N, and the pressure measurements integrated over the compression surface $F_p \approx 84$ N.

Starting Tests

The starting mechanism of intakes in pulse facilities such as the gun tunnel is different from the quasi-steady starting mechanism of intakes in flight. Non-self-starting intakes can be started in the unsteady processes of the gun tunnel when the initial test-section vacuum is sufficiently high. The REX1020 intake was tested in QinetiQ's High Density Tunnel (HDT) to confirm it was self-starting. The HDT operates as a Ludwieg tube with a valve that gradually opens over a period of 20 ms. It has been demonstrated that axisymmetric internal compression intakes do not start in the facility if the contraction ratio is greater than the Kantrowitz limit.

The REX1020 intake started in the HDT when tested at high Reynolds numbers over the range $4.63 \times 10^6 < Re_D < 5.68 \times 10^6$ with $T_w/T_{01} \approx 0.7$.

Conclusions

Reexpansion intakes have very low cowl drag at the expense of decreased efficiency and nonuniform exit flow. Scramjet engine performance increases monotonically with the amount of isentropic compression for intakes of this type. An optimum flow-turning angle is only found in the case when the external compression occurs exclusively through a single shock wave. Calculated stream-thrust-averaged performance parameters for the REX1020 intake were considerably higher than measured when isolator skin friction was excluded from the analysis. This effect is sufficiently large that the value of the wind-tunnel data is greatly decreased if the intake model isolator is not a replica of the engine isolator. Viscosity also results in reduced contraction ratio (and lower performance) as the design must account for significant boundary-layer displacement at the intake throat. The dominance of viscous effects on hypersonic intake performance and operability (starting and flow separations) means that the intakes must be tested at flight Re_D, T_w/T_{01}, and with all boundary-layer management devices such as trips and steps in place.

References

[1]Carlson, C. H., "Preliminary Scramjet Design for Hypersonic Airbreathing Missile Application," NASA CR 3742, Nov. 1983.

[2]Mölder, S., and Romeskie, J. M., "Modular Hypersonic Inlets with Conical Flow," *Hypersonic Boundary Layers and Flow Fields*, CP-30, AGARD, May 1968.

[3]Van Wie, D. M., "Scramjet Inlets," *Scramjet Propulsion*, edited by E. T. Curran and S. N. B. Murthy, Progress in Astronautics and Aeronautics, Vol. 189, AIAA, Reston, VA, 2000, pp. 447–511.

[4]Eckert, E. R. G., "Engineering Relations for Friction and Heat Transfer to Surfaces in High Velocity Flow," *Journal of Aeronautical Sciences*, Vol. 22, No. 8, 1955, pp. 585–587.

[5]Van Driest, E. R., "The Problem of Aerodynamic Heating," *Aeronautical Engineering Review*, Vol. 15, No. 10, 1956, pp. 26–41.

[6]Stollery, J. L., "Supersonic Turbulent Boundary Layers: Some Comparisons Between Experiment and a Simple Theory," *Aeronautical Quarterly*, Vol. 28, No. 2, May 1976, pp. 87–98.

[7]Kantrowitz, A., and Donaldson, C., "Preliminary Investigation of Supersonic Diffusers," NACA WR L-713, May 1945.

[8]Curran, E. T., and Bergsten, M. B., "Inlet Efficiency Parameters for Supersonic Combustion Ramjet Engines," U.S. Air Force Aero Propulsion Lab. Rept. APL TDR 64-61, Wright–Patterson Air Force Base, OH, June 1964.

[9]Billig, F. S., and Van Wie, D., "Efficiency Parameters for Inlets Operating at Hypersonic Speeds," *8th International Symposium on Air Breathing Engines*, ISABE 87-7047, AIAA, New York, 1987, pp. 118–129.

[10]Mölder, S., and McGregor, R. J., "Analysis and Optimization of Scramjet Inlet Performance," *17th Congress of the Aeronautical Sciences*, International Council of the Aeronautical Sciences, Stockholm, Sept. 1990, pp. 1328–1339; also ICAS Paper 90-4.7.3, 1990.

[11]Andreev, V., and Penzin, V., "Some Aspects of Scramjet Vehicle Integration," *Scramjet Propulsion*, edited by E. T. Curran and S. N. B. Murthy, Progress in Astronautics and Aeronautics, Vol. 189, AIAA, Reston, VA, 2000, pp. 337–353.

[12]Cain, T., and Walton, C., "The Sustained Hypersonic Flight Experiment," AIAA Paper 2003-7030, Dec. 2003.

[13]McBride, B., and Gordon, S., "NASA-Lewis Chemical Equilibrium Program CEA," NASA RP-1311, Part I, 1994 and NASA RP-1311, Part II, 21 Oct. 1996.

[14]Buttsworth, D. R., and Jones, T. V., "A Fast-Response Total Temperature Probe for Unsteady Compressible Flows," American Society of Mechanical Engineers, Paper 96-GT-350, June 1996.

[15]Feindt, E. G., "Untersuchungen über die Abhängigkeit des Umschlages Laminar-Turbulent von der Oberflächenrauhugkeit und der Druckverteilung," Ph.D. Dissertation, Braunschweig, Germany, 1956.

[16]Schneider, S. P., "Hypersonic Laminar-Turbulent Transition on Circular Cones and Scramjet Forebodies," *Progress in Aerospace Sciences*, Vol. 40, Feb. 2004, pp. 1–50.